Original Research Article

GREENHOUSE GASES SCIENCE AND TECHNOLOGY

CO_2-water-rock interactions in undeformed and sheared claystone caprocks from Northern Europe

Roland Vernooij, Vrije Universiteit Amsterdam, Amsterdam, The Netherlands
Tiago de Abreu Siqueira, Pontifical Catholic University of Rio Grande do Sul (PUCRS), Porto Alegre, RS, Brazil
Suzanne Hangx and Christopher Spiers, Utrecht University, Utrecht, The Netherlands
Marcelo Ketzer, Linnaeus University, Kalmar, Sweden
Rodrigo Sebastian Iglesias, Pontifical Catholic University of Rio Grande do Sul (PUCRS), Porto Alegre, RS, Brazil

Abstract: One of the most promising, cost-effective, and readily available technologies for reducing greenhouse gas emissions to the atmosphere is the capture and separation of CO_2 from large stationary sources and storage in geological formations. Storage security, especially in the early stages of operation, is mostly guaranteed by caprock formations with very low permeability overlying the reservoir, capable of containing the injected fluid. Chemical alterations of the formation brine, caused by CO_2 injection may cause dissolution and precipitation of secondary minerals, potentially increasing the risks of leakage from the reservoir. In order to evaluate these processes and their potential to induce the formation of leakage pathways in ultrafine fault gouges, a series of batch experiments was performed on crushed and sheared samples from three different caprock formations from Northern Europe (Sollingen, Röt and Opalinus claystones). The experiments were supported by numerical models of the kinetics of mineral dissolution and precipitation simulating the same experimental conditions, and over a longer time (10 000 years). Minor mineral alterations were observed after the batch experiments, the most important being: illite dissolution for the Opalinus and Röt formation samples, and dolomite dissolution and the transformation of illite and chlorite into kaolinite for the Sollingen sample.

Additional supporting information may be found online in the Supporting Information section at the end of the article.

Keywords: caprock; water-rock interaction; CCS; shear fracture

Correspondence to: R. S. Iglesiias, Institute of Petroleum and Natural Resources (IPR), Pontifical Catholic University of Rio Grande do Sul (PUCRS) – Av. Ipiranga 6681, Building 96J, Porto Alegre – RS, Brazil.
E-mail: rodrigo.iglesias@pucrs.br
Received August 7, 2020; revised November 16, 2020; accepted November 25, 2020
Published online at Wiley Online Library (wileyonlinelibrary.com). DOI: 10.1002/ghg.2045

Introduction

Carbon capture and storage (CCS) is considered one of the most promising solutions to reduce CO_2 emissions to the atmosphere.[1,2] Geological formations such as deep saline aquifers, deep coal seams, and petroleum fields are suitable reservoirs for long-term storage of CO_2 captured from large stationary sources. The occurrence of natural CO_2 fields such as the Mc Elmo dome and Sheep Mountain in Colorado and the Bravo dome in New Mexico[3] demonstrate that geological formations can safely store large quantities of CO_2 for millions of years.[4] One of the major barriers for large scale implementation of CO_2 storage in geological media is the demonstration of CO_2 confinement in the reservoir. In particular, onshore contamination of aquifers is regarded a major concern, as the acidifying effect of CO_2 into water could promote the mobilization and transport of trace metals and bitumen to groundwater aquifers.[5,6]

Understanding CO_2-water-rock interactions in reservoir and caprocks is of great importance because mineral dissolution can create pathways for CO_2 leakage through the caprock. In spite of that, few studies focus on the CO_2-water-rock interactions in caprocks and deformed (sheared) caprocks,[7–15] as most of the research is devoted to the understanding of alteration within reservoirs.[7,10,16–20]

Previous studies show that sheared (fractured) components may react differently than the undeformed caprock and facilitate CO_2 leakage from reservoirs. Fracturing not only may lead to an increase in porosity and permeability (facilitating CO_2 penetration), but also the shearing movement may lead to grain size reduction, causing the material to react faster.[21]

The aim of this study was to evaluate and compare, via batch experiments and numerical modeling, the mineral alterations in sheared and undeformed samples of clay-rich caprock formations from Northern Europe after exposure to a CO_2-rich brine. The caprock formations were selected based on their potential suitability to function as a seal for geological storage of CO_2 and likeliness to react within the experimental timeframe. All locations addressed in this research have been presented as possible storage sites for CO_2 due to their favorable properties and accessibility.

Results of this work will contribute to a better understanding of leakage scenarios of CO_2 in claystone caprocks such as those in the Weyburn CCUS-EOR project (Midale Fm.).

Geological setting of samples

Sollingen claystone and Röt claystone (offshore, Netherlands)

Figure 1 shows the stratigraphy, group and formation names, stages, and sequences in the southern North Sea region.[22] The Triassic sediments of the P18-4 gas field can roughly be subdivided in the late lower Germanic Trias group and the upper Germanic Trias group. The boundary between the two groups is formed by the Hardegsen or base Sollingen unconformity. Directly above the unconformity lie the Sollingen and Röt clay stones and evaporites. Deposited in a lacustrine setting, the Sollingen consists of red, green, and locally grey claystones. On the location of the samples, it has a thickness of approximately 10 m. The overlying Röt Formation consists of thin-bedded claystones and is approximately 40 m thick.[23]

Röt claystone and Sollingen formations form the primary and secondary seals, respectively, of the P18-4 gas field. The depleted P18-4 gas field was one of the fields selected for CO_2 storage as part the European demonstration projects under the European Energy Programme for Recovery.[23] Though the project has been cancelled, the storage complex remains representative for many potential CCS sites in Europe and particularly the North Sea.

Opalinus Claystone (Switzerland)

The Opalinus Clay is around 180 million years old (Triassic to Jurassic age). The name is derived from the Leioceras Opalinum, a particular ammonite whose shell consists of aragonite. The Opalinus clay formation was deposited over a deposition period of around 400 000 years in a shallow sea environment with an average water depth of 20–50 m.[24] The shallow sea was bordered by the Rheinish state mountains in the north, the Alemannic islands in the south and the Bohemian massif in the east. The deposition zone roughly covers the area between the cities of Bern, Munich, and Strasbourg.

At Mont Terri in the north-west of Switzerland, the Opalinus Clay Formation was first studied in 1989 jointly by the Swiss Geological Survey (SNHGS, now the Federal Office for Water and Geology – FOWG) and NAGRA (the Swiss National Cooperative for the Disposal of Radioactive Waste), during construction of a reconnaissance tunnel. The Opalinus Clay occurs in this region as a 100- to 120-m-thick subhorizontal

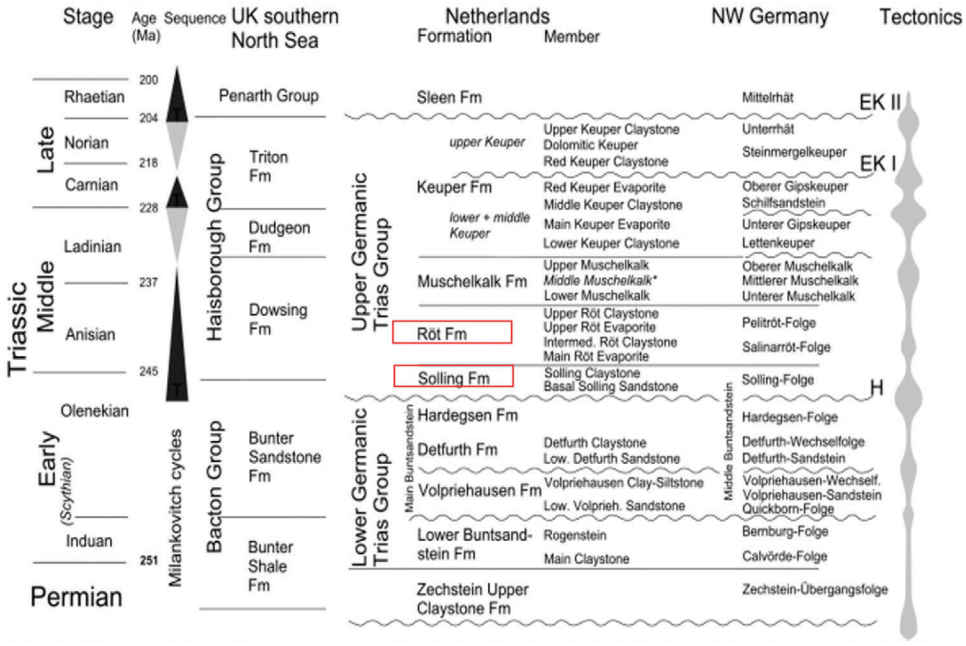

Figure 1. Overview of group and formation names present in P18 gas field along with associated depth intervals from the vertically drilled P18-02 well (Formations studied are highlighted in red). Transgressive sequences are drawn in black, regressive sequences in grey. EK I, main Early Kimmerian Unconformity, base Norian; EK II, Early Kimmerian II Unconformity, base Rhaetian; H, Hardegsen Unconformity. Middle Muschelkalk comprises of the Muschelkalk Evaporite and Middle Muschelkalk Marl.[22]

layer in a nearly undisturbed tectonic setting, and the samples were obtained from a borehole.[25]

Methodology

The study was divided in two parts. The first part aims to determine what alterations take place in the caprock in the presence of CO_2-saturated brine. Autoclave batch experiments were performed on crushed undeformed material from the selected formations (see Section on geological setting of samples). In addition, geochemical modeling software PHREEQC was used to calculate the kinetics of mineral dissolution and precipitation during the experiment, as well as on a longer geological timescale.

The second part focusses on determining whether mineral reactivity with the CO_2-rich brine is affected within the extremely fine shear band due to variations in grain size and fluid flow through the shear. A recently developed method was used for preparing samples with intact, thin bands of fault gouge.[12] This section describes the methodology employed for the experiments, characterization, and numerical modeling performed in this study.

Samples

Both the Sollingen and the Röt claystone samples originate from the same well (P18-02) at different depths. Representative samples were taken from the Triassic Sollingen at a depth of 3292 m below seafloor and for the Röt at a depth of 3290 m below seafloor.[12] The Opalinus clay samples were obtained from the underground tunnel that crosses the formation at the Mont Terri Rock Laboratory.[26]

Mineral composition

The rock samples were characterized in terms of their morphology and chemical composition, before and after the experiments, by scanning electron microscopy coupled with energy dispersive X-ray spectroscopy (SEM-EDS), a technique that allows visualizing the mineral phases of the samples at microscale, as well as obtaining a semiquantitative characterization of the sample. X-ray diffraction (XRD), which provides the mineral phase composition from the analysis of the crystalline reticulum of the sample, was also employed in the characterization.

Table 1. Mineral composition of the studied samples, as determined by X-ray diffraction (Figures S1, S3, and S5).

	Sollingen (%)	Röt (%)	Opalinus (%)
Quartz	5	66	44
K-Feldspar		10	
Albite		5	
Kaolinite		4	24
Calcite			16
Dolomite	85		
Illite	5	7	8
Clinochlore	5	7	8

Table 2. Saline solution compositions ($mg.kg^{-1}$ solution) used in batch experiments.

	Sollingen[1]	Röt [1]	Opalinus [2]
Na^+	50 600	50 600	6 896
Cl^-	87 900	87 900	10 635
Mg^{2+}	970	970	
Ca^{2+}	8 000	8 000	

[1] 12
[2] 28,29

Brine characterization

The characterization of the brine was carried out by Inductively Coupled Plasma Optical Emission Spectrometry (ICP-OES), providing quantification of selected cations in solution. With this analyses, coupled with rock characterization, it was possible to identify products of dissolution or variations in the concentration of the elements indicating precipitation.[27]

Mineral compositions of the caprocks and brine

XRD analyses were carried out on the collected samples. The compositions obtained are shown in Table 1.

To mimic the *in situ* conditions present in the reservoir, a synthetic saline solution with similar composition as the pore fluid of the respective underlying reservoirs. The brine compositions as used in the experiments are shown in Table 2:

The brines were synthesized using pure salts and Milli-Q water with a resistivity of 18.2 $M\Omega.cm^{-1}$ at 25 °C.

Crushed powder samples

As the amount of direct shear-tested material was too small for XRD analysis, and it is important to preserve the shear band structure, pre- and postreaction XRD characterization was performed on the crushed powder used in the batch experiments. Rock samples obtained from the different formations were crushed before experiment in order to enhance and homogenize the overall reactivity.

Sheared plate samples

The direct shear tests have been performed following the method described in detail by Samuelson and Spiers.[12]

The sheared material comes in the form of roughly 1 mm thick plates (Fig. 2a). To keep the plates from separating, two PTFE blocks of roughly 20 × 32 × 2 mm are placed on both sides of the material. Small holes (1 mm in diameter) are drilled in the Teflon plates to allow the CO_2-saturated brine to react with the rock surface (Fig. 2b). The construction is enclosed by an inert FEP shrink tube. The sides of the sample are closed off with inert PTFE tape. The shrink tube was punctured with 1 mm diameter holes on both sides to ensure accessibility of the fluid to the sample.

Autoclave experiments

Figure 3 shows a schematic view of the experimental setup. Two experiments were carried out simultaneously, using two 75 mL Hastelloy-C276 pressure vessels (Parr Instruments, USA). The temperatures were measured inside the reaction vessel. Two reactor controllers (Parr Instruments, type 4838) were used in combination with resistance heaters enclosing the reaction vessel to ensure constant temperature of 100 °C.

In geochemical batch experiments under laboratory conditions, the sample material is often exposed to an excess of reaction fluid. First, to ensure complete submersion of the sample, but also to favor mineral dissolution with far-from-equilibrium conditions. Here, a 5:1 brine to sample ratio was used, similar to previous similar studies.[30–32] For the experiments with the crushed material a total sample mass of 6 g of

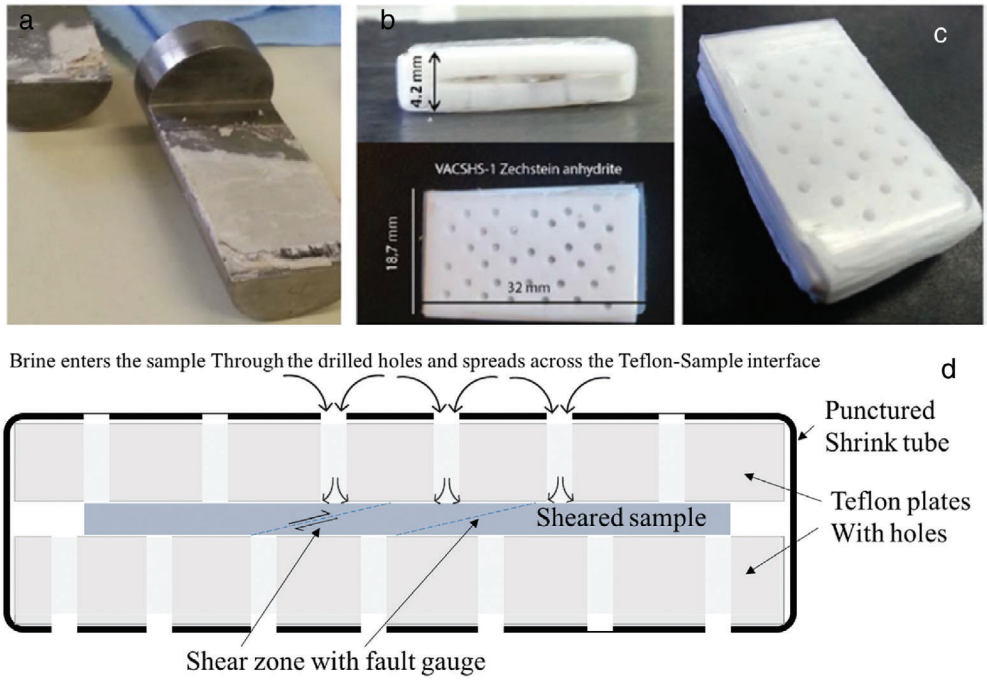

Figure 2. Sample preparation: (a) Sample material after dry shearing, (b) sandwiched between two inert Teflon plates and FEP shrink tube, and (c) sides covered with Teflon tape. (d) Schematic side-view of the sheared sample plate holder.

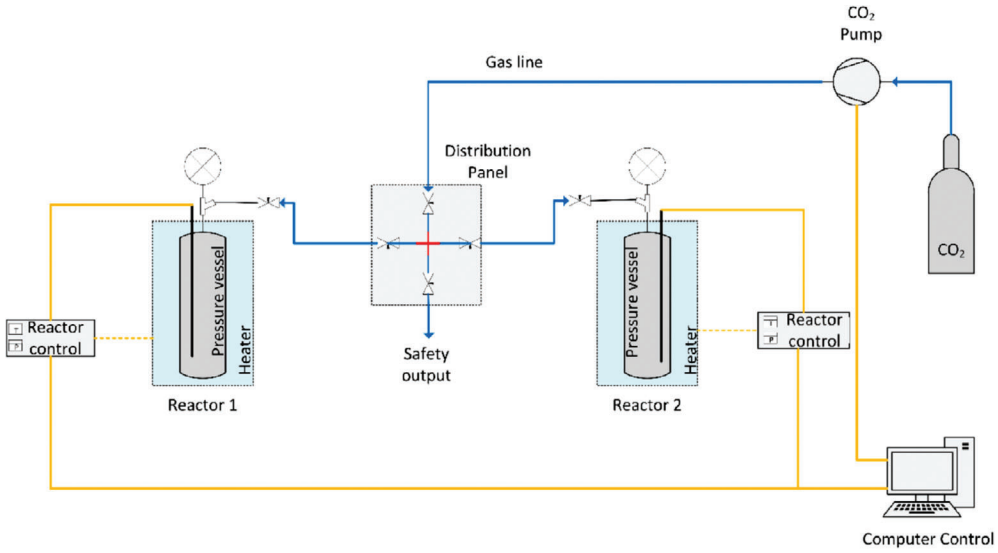

Figure 3. Schematic view of the experimental setup for the autoclave experiments.

crushed caprock was reacted with 30 mL of brine. For the sheared samples 20 mL of brine were used, as this is minimum amount to keep the plate sample fully submerged. The autoclaves were pressurized to 10 MPa with CO_2, and repressurized until the pressure no longer dropped due to CO_2-dissolution in the brine. The experiments were carried out for 21 days.

Modeling

The PHREEQC geochemical modelling software[33] was used to simulate the kinetics of dissolution and precipitation during the experiment (21 days) and over a larger timescale (10 000 years). Mineral properties were obtained from the LLNL database, which is included in the software, freely available from the

USGS website. The mineral formation composition that was used as input for the model was the composition obtained by X-ray diffraction analysis (Table 1). Initial solution compositions used in the models were based on those presented in Table 2.

All minerals present in the sample were considered as kinetic reactants, and are considered to react according to the generalized transition-state theory-based rate law,[34] in the improved format proposed by Palandri and Kharaka,[35] with specific acid, neutral and basic-catalyzed mechanisms and their respective parameters (Eqn (1)).

$$\text{Rate} = \text{SSA} \cdot \left(k_{\text{acid}}^{298.15\ K} \cdot e^{-\frac{E_{\text{acid}}}{R}\left(\frac{1}{T}-\frac{1}{298.15\ K}\right)} a_{H^+}^{n_{\text{acid}}} + k_{\text{neutral}}^{298.15\ K} \cdot e^{-\frac{E_{\text{neutral}}}{R}\left(\frac{1}{T}-\frac{1}{298.15\ K}\right)} + k_{\text{basic}}^{298.15\ K} \cdot e^{-\frac{E_{\text{basic}}}{R}\left(\frac{1}{T}-\frac{1}{298.15\ K}\right)} a_{H^+}^{n_{\text{basic}}} \right) \cdot (1 - \text{SR}) \quad (1)$$

Parameters for each mineral for Eqn (1) (SSA: specific surface area; *k*: acid, netural and basic rate constants; *E*: acid, neutral and basic activation energy; *n*: acid and basic reaction order and *SR*: saturation ratio—the ratio between ion-activity product and equilibrium constant) are presented in Table 3. Numerical modeling input files are included as Supporting Information to this article.

A simulation for the whole experiment with each sample was performed, with the following steps: (1) equilibration of solution with CO_2 at atmospheric conditions; (2) equilibration of CO_2 with solution, while heating from 25 to 100 °C; (3) reaction kinetics with CO_2 at 100 bar partial pressure and 100 °C for 21 days, and (4) cooling and depressurization, from 100 to 25 °C and 100–1 bar, respectively, for 6 hr. Additional simulations for 10 000 years were also performed, starting with the equilibrated solution at 100 °C, and keeping CO_2 partial pressure at 100 bar for 10 000 years (no depressurization step was included in this case).

The initial mineral amounts (in moles) were calculated from the mineral composition percentage (equivalent to volumetric fraction), density, molecular weight and mass of the sample, and are also presented in Table 3. Some selected secondary minerals were included in the simulations (with zero initial amount), based on the calculated saturation indexes after step 2 (equilibration of the system with CO_2 at 100 °C).

Results

In this section, the mineral alterations found in the batch experiments with the undeformed (crushed powder) samples and the shear plates will be presented, followed by the numerical simulation results.

Undeformed samples

Opalinus

The initial Opalinus claystone contained a relatively high amount of quartz (44%), with major components including kaolinite (24%), calcite (16%), clinochlore (8%), and illite (8%). The composition found in this study differs from the composition of the larger formation found by,[21] which presents a much lower quartz (28%) and higher calcite content (25%).

Figure 4 shows the Opalinus clay powder fraction before (A) and after the experiment (B). The initial powder consisted of larger sub-angular fractions that either fully consisted of clay or were covered in clay particles. After reaction, the overall textural aspect of the sample remains, although the smaller fragments covering the bigger grains now appear to be more platy showing clear signs of layering.

ICP-OES analysis shows increases in Ca^{2+} and Mg^{2+}, and appearance of K^+ in solution after the experiment, which is more pronounced with the crushed sample (Table 4). This increase is mostly due to some dissolution of calcite and illite from the sample. The occurrence of potassium is a clear indication of illite dissolution, as it is the only source of this element in the sample.

Sollingen

The Sollingen claystone mainly consists of dolomite (85%) with minor fractions of illite, clinochlore, and quartz (all ca. 5%, Table 1), also deviating significantly from previously reported composition,[12] which presented nearly half the amount of dolomite (43%) and much higher illite content (46%). No signs of kaolinite or K-feldspar were found in the initial material in either XRD or SEM analyses (although XRD may not detected K-feldspars if it is present in low amounts). The initial Sollingen powder consists of rounded to subangular grains, covered with a layer of extremely fine-grained platy material.

Energy-dispersive spectroscopy (EDS) scanning showed high amounts of Al, Si among other minor

Table 3. Mineral data and parameters for numerical modeling.

	Initial amount (mmole)							
Mineral	Solligen	Röt	Opalinus	SSA ($m^2.g^{-1}$)	Mechanism	Log K (25 °C) (log $mol.m^{-2}.s^{-1}$)	E_a ($J.mol^{-1}$)	n (for a(H+))
Quartz	5.09	66.22	43.76	0.0225[a]	neutral	−13.99	87 700	–
K-feldspar	–	2.09	–	0.5[b]	acid	−10.06	51 700	0.5
					neutral	−12.41	38 000	–
					basic	−21.2	94 100	−0.823
Albite	–	1.15	–	0.02[c]	acid	−10.16	65 000	0.317
					neutral	−12.56	65 000	–
					basic	−15.6	71 000	−0.572
Kaolinite	–	0.92	5.51	20[c]	acid	−11.31	65 900	0.777
					neutral	−13.18	22 200	–
					basic	−17.05	17 900	−0.472
Calcite	–	–	18.63	0.15[c]	acid	−0.3	14 400	1
					neutral	−5.81	23 500	–
					basic	−3.48	35 400	1
Dolomite	27.56	–	–	0.18[c]	acid	−3.76	56 700	0.5
					neutral	−8.6	95 300	–
					basic	−5.37	45 700	0.5
Illite	0.81	1.11	1.24	41[d]	acid[f]	−11.72	46 000	0.6
					neutral[f]	−15.05	14 000	–
					basic[f]	−12.31	67 000	−0.6
Clinochlore	0.53	0.73	2.43	0.1[b]	acid	−11.11	88 000	0.5
					neutral	−12.52	88 000	–
Smectite	–	0.15	1.17	61[d]	acid	−10.98	23 600	0.34
					neutral	−12.78	35 000	–
					basic	−16.52	58 900	−0.4
Muscovite	–	–	–	0.68[c]	acid	−11.85	22 000	0.37
					neutral	−13.55	22 000	–
					basic	−12.31	22 000	−0.6
Dawsonite	–	–	–	11.5[e]	acid[g]	−4.5	63 820	0.98

[a] 36; [b] 37; [c] 38; [d] 39; [e] 40; [f] 41; [g] 42

elements, suggesting the grains are coated with clay minerals. After reaction, the extremely high salinity of the formation brine has led to the precipitation of some halite crystals after opening and drying of the sample.

As in the case of the Opalinus sample, ICP-OES analyses show increases in the concentrations of both Ca, K, and Mg in solution (Table 5). In this case, the increase is possibly coming from the dissolution of

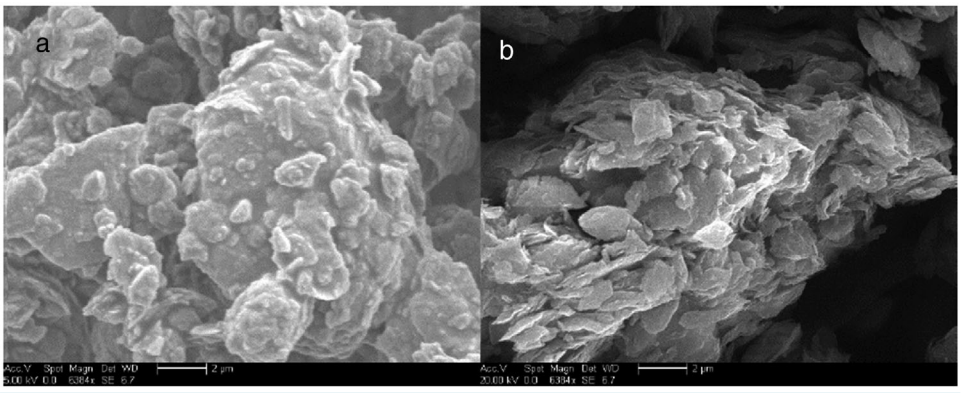

Figure 4. SEM images of crushed Opalinus clay, prior to (A) and after CO_2 + brine reaction (B).

Table 4. Dissolved ion concentrations (ppm) in the brine for the autoclave experiments of Opalinus clay samples obtained by analysis of ICP-OES for cations, and IC for anions.

	Ca	Na	K	Mg	Cl^-
Initial	–	6 810 ± 0.9	–	–	12 518 ± 0.5
Crushed	135 ± 1.8	6 545 ± 2.7	191 ± 0.8	304 ± 0.7	12 653 ± 0.5
Sheared	65 ± 1.0	4 801 ± 24	23 ± 1.0	14 ± 1.0	12 305 ± 0.5

Table 5. Dissolved ion concentrations (ppm) in the brine for the autoclave experiments of Sollingen clay sample obtained by analysis of ICP-OES for cations, and IC for anions.

Sollingen	Ca	Na	K	Mg	Cl^-
Initial	6 811 ± 0.7	38 630 ± 5.0	–	860 ± 16.4	96 945 ± 0.5
Crushed	8 428 ± 2.5	37 070 ± 1.3	1 475 ± 2.9	1 271 ± 13.1	99 804 ± 0.5
Sheared	8 373 ± 1.0	36 390 ± 1.1	103 ± 0.8	1 059 ± 0.7	102 673 ± 0.5

Table 6. Dissolved ion concentrations in the brine for the autoclave experiments of Röt claystone samples obtained by analysis of ICP-OES for cations, and IC for anions.

Röt	Ca	Na	K	Mg	Cl^-
Initial	7 378 ± 2.4	38 630 ± 2.5	–	860 ± 1.9	96 945 ± 0.5
Crushed	7 778 ± 1.9	38 008 ± 1.6	1 495 ± 2.8	1 327 ± 1.1	96 495 ± 0.5

some of the dolomite and the illite content during the experiment.

Röt claystone

Like the Opalinus claystone, the Röt Formation also contained a very high amount of quartz (66%), in addition to potassium feldspar (10%), illite (7%), clinochlore (7%), albite (5%), and kaolinite (4%). Previously reported composition shows a much lower quartz (35%) and higher illite (55%) content.[43] The analyzed sample is composed of subangular grains showing great variation in sizes.

Postexperiment ICP-OES results show an increase in Ca, K, and Mg in the aqueous solution (Table 6). Possible sources for these are the dissolution of some calcite and illite during reaction. As was the case in the Sollingen experiment, halite crystal precipitated after the experiment due to the extreme salinity of the brine.

Sheared samples

After the reaction was finished, the sheared sample casings were opened. In the case of the Opalinus claystone, the outer side of both sample plates (which is not directly in contact with the sample) was covered

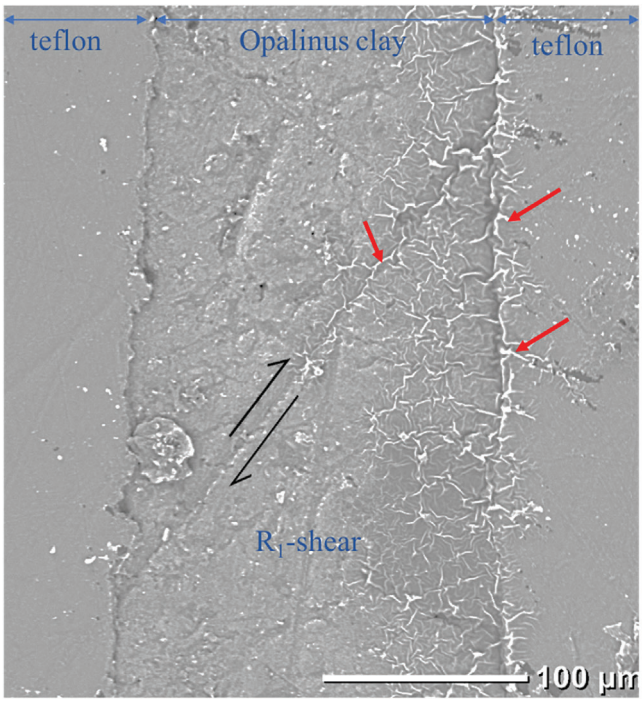

Figure 5. Shear band (blue ellipse), identified as R1-shear in Opalinus clay sample obtained by SEM-EDS after CO_2-brine reaction. In the right side, red arrows show a network of flow channels.

with a reddish-brown material upon retrieving the samples. This did not originate from the brine and was only found on the outside of the plates. As expected, the increase in concentration of Ca^{2+} and Mg^{2+} after the experiments is lower than with the crushed samples, as less mineral surface is available for reaction (Tables 4 and 5).

Various shear bands were observed within the samples. Figure 5 shows a shear band (blue ellipse), identified as R_1, and observed in the Opalinus 2 clay sample after CO_2-brine reaction analyzed by EDS. The boundary on the right side of the picture clearly shows a network of flow channels (red arrows). As would be expected, the majority of the precipitation took place along the Teflon/sample interface as this would be the most easily accessible for the brine. Also, this region might have held fine grained material originating from a shear boundary. From the main channel, side channels of precipitated material enter into the sample and to a minor extent, into the Teflon on the right side. The precipitation of silicon clearly shows that the shear band has acted as a preferential pathway for the brine-CO_2 to enter. Following the exact shape of the shear band, the brine appears to have penetrated significantly into the sample.

Figure 6B and 6D shows more detailed maps of EDS of the first part of the shear band with the corresponding elemental maps for silicon. Although all the signal peaks were identified, no element showed significantly increased presence in the precipitates within the sample. In the PTFE however, situated on the right side of the vertical shear zone, the precipitates are clearer and seem to contain silicon as is shown in Figure 6, where the maps are represented by a color grading from dark blue to white, being that these colors represent the relative density of silicon atoms.

Figure 7 shows a possible shear band identified in this sample. As the band with the larger angle to the PTFE (Fig. 7A) did not show any signs of grain size reduction and appeared to be consistent with a mark on the Teflon, this was identified as a scratch from the grinding process. Figure 7B shows the elemental map for carbon (red) and oxygen (green) of the area surrounding the band.

The same behavior observed in the Fig. 7, was observed in a different shear zone in the Opalinus clay sample (Fig. 8). All the spectral peaks detected by the EDS were successfully identified. In both cases, major clay mineral forming elements like oxygen, silicon, potassium, and aluminum showed a decreased presence in the shear band while there was a higher presence of carbon, possibly from the epoxy resin used in the sample preparation. Furthermore, no increased presence of either calcium, magnesium, iron, or sodium was detected hence, no secondary carbonates or salts precipitated in the shear band.

Another possible shear band was observed within the Sollingen sheared plate Fig. 9. Besides the R1-shear band located in the middle, another possible boundary shear band was found at the Teflon/sample interface.

Elemental maps were created from a close up on the center of the shear region (Fig. 10).

The yellow parts in Fig. 10B show grains of dolomite where calcium and magnesium overlap. The grains appear to be surrounded by a matrix of smaller clay particles. The large white spot on the map is a result of static overcharging of the sample where the material was insufficiently grounded. EDS analysis of the supposed shear region shows a high silicon density in the band. From the analysis it is not possible to see signs of mineral precipitation or dissolution.

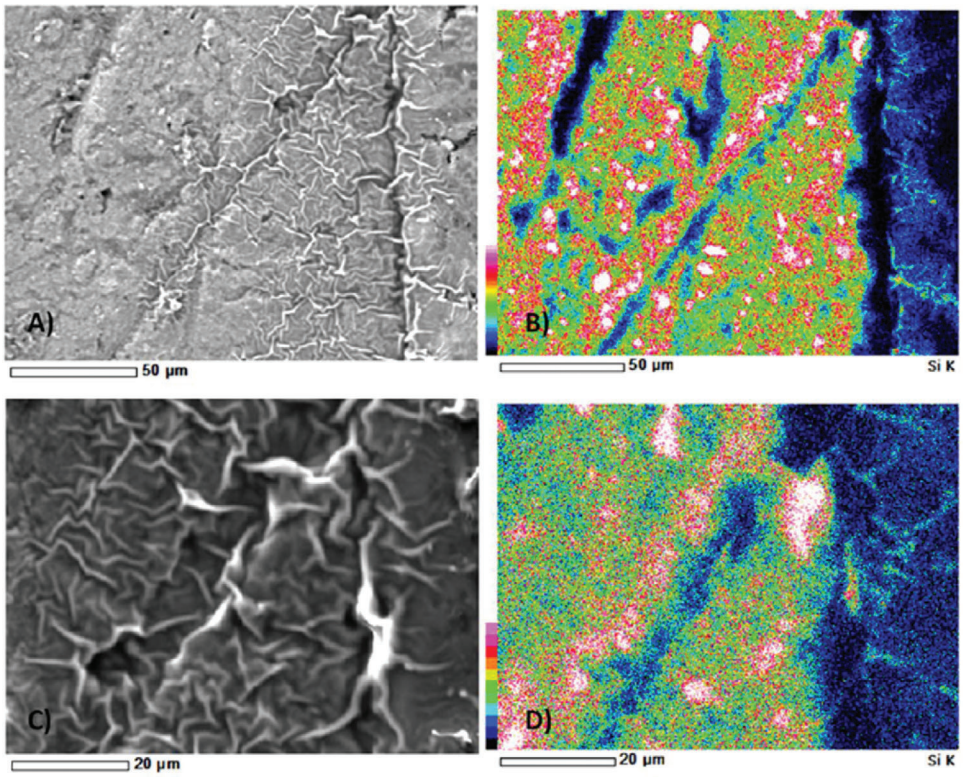

Figure 6. Magnified map of the precipitated minerals in the fracture (A,C) and corresponding elemental map for silicon (B, D respectively). The colour scale shown on the left side of the EDS images indicates the abundance of Si, with black indicating no Si, while white indicates the maximum abundance of Si in the image.

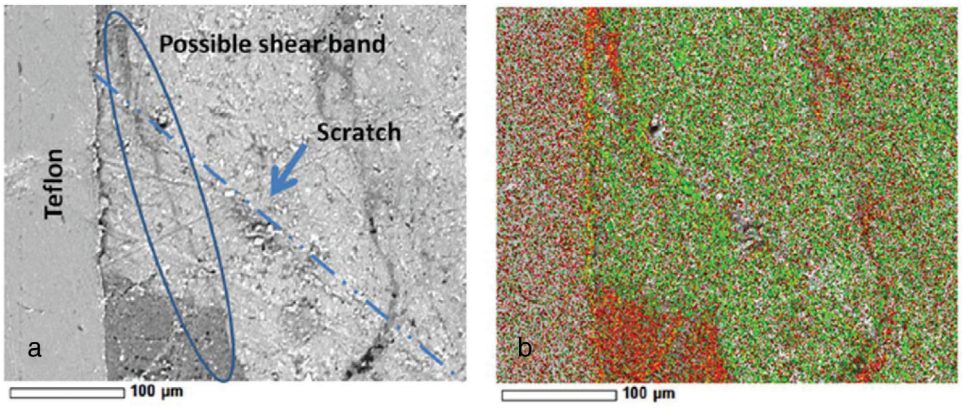

Figure 7. Backscattered electron map of a possible shear zone (blue ellipse) and a possible scratch identified by the dashed line in the Opalinus 2 sample (A), Elemental map of the corresponding area for carbon (red) and oxygen (green).

Numerical modeling

Result from the simulations of kinetics of dissolution and precipitation of minerals are presented first for the experiment time (21 days) and later for the longer timescale runs (10 000 years).

Simulation of experiments (21d)

Table 7 presents the amounts of Ca, Mg, K, Si, and Al elements and carbonate/bicarbonate species in the initial solution (after equilibration with atmospheric CO_2) and after the experiment (following

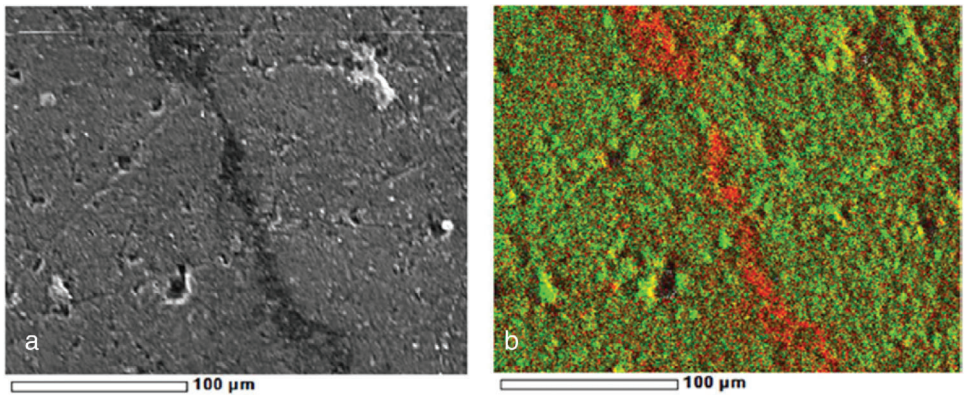

Figure 8. Secondary electron map of a proposed shear band in the Opalinus 2 sample (A) Elemental map of the corresponding area for carbon (red) and oxygen (green).

Table 7. Calculated pH and concentration of selected elements and species in solution before (initial) and after 21 days reaction (final) with rock sample and CO_2.

Sample		Log concentration (mol.kg^{-1})							
Sollingen	pH	Ca	Mg	K	Si	Al	HCO_3^-	CO_3^{2-}	CO_2(aq)
Initial	5.47	−0.73	−1.45	0.00	0.00	0.00	−5.73	−9.92	−5.18
Final	7.21	−0.73	−1.45	−4.39	−3.12	−8.74	−3.99	−6.43	−5.18
Röt									
Initial	5.47	−0.73	−1.45	0.00	0.00	0.00	−5.73	−9.91	−5.18
Final	6.78	−0.73	−1.46	−3.64	−3.62	−8.37	−4.14	−7.29	−5.18
Opalinus									
Initial	5.58	0.00	0.00	0.00	0.00	0.00	−5.60	−9.91	−5.00
Final	8.36	−3.44	−5.81	−3.04	−2.84	−4.82	−3.32	−4.51	−5.51

depressurization of the system, i.e., pCO_2 restored to atmospheric values).

Solution compositions show more pronounced changes in compositions, especially when the species are not initially present in the system, appearing after the reaction period due to some mineral dissolution (for example, Al, K, and Si in the Sollingen sample reaction). After the complete experimental cycle (heating/pressurization, reaction, and cooling/depressurization), the pH increased in all cases. However, while the system is under CO_2 pressure, pH decreased to acidic values—4.2, 3.5, and 4.8 for the Sollingen, Röt, and Opalinus sample reaction, respectively. The lower value for the Röt case is expected as this sample does not have carbonate minerals that can buffer the solution pH.

Figure 11 shows the variation in the rock mineral amounts that take place during the 21-day reaction period, simulated by the kinetic modeling. As expected, these variations are quite small (always lower than 0.04 mmol). However, some trends of the more pronounced changes observed in the long-term simulations are already noticed. Illite dissolution occurs in all samples, resulting in an overall increase in Al, K, and Si in solution, partially offset by some kaolinite and chlorite (clinochlore) precipitation.

Carbonates, when present, do not dissolve as much as would be expected in an acidic medium generated by a high CO_2 partial pressure. In the Sollingen and Röt samples, this is due to the high initial calcium content in solution and a pH increase after depressurization. In the Opalinus sample, the initial solution does not have calcium, and calcite is significantly dissolved (going from 9.77 to 9.00 mmole, ca. 9%) during the 21-day reaction period, while CO_2 partial pressure is high and pH becomes more acidic (ca. 4.8). However, after cooling and depressurization, pH increases to 8.5 and

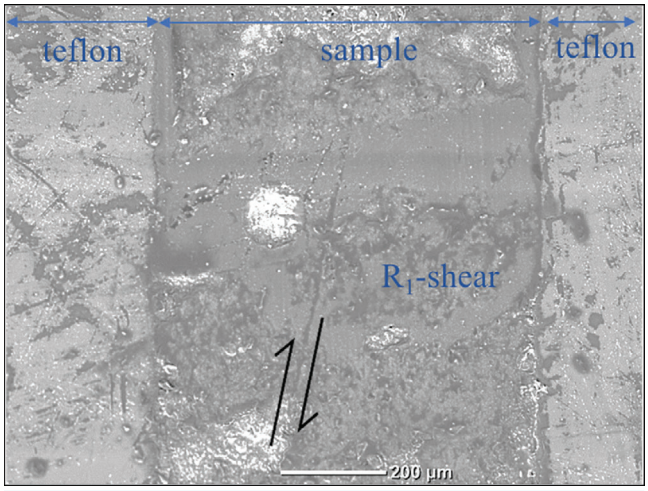

Figure 9. Proposed shear zone in the sheared Sollingen sample.

calcite is re-precipitated almost to the initial amount, resulting in less than 0.01 mmol variation.

Figure 12 shows the variation of the aqueous solution properties—pH, selected cations and CO_2 (aq) concentration—and mineral amounts during a 10 000-year kinetic simulation.

In 10 000 years, none of the rock compositions studied appear to reach a complete equilibrium. Overall, the alterations are quite similar for the three rocks, and follow the trends indicated by the short-term (21 days) simulations: illite is extensively dissolved (complete for the Röt and Opalinus claystones) while chlorite (clinochlore) dissolves slowly and continuously, not reaching an equilibrium in 10 ky, resulting in formation of mostly K-feldspar and kaolinite. The Sollingen claystone is the least altered of the rocks in the simulations. Besides the above mentioned alterations, some dolomite is also formed steadily, reaching 2.88 mmol at the end—a ca. 5% increase from the initial amount (2.71 mmol). This increase in dolomite is not enough to absorb all the Mg released from illite and clinochlore dissolution, whose amount in solution increases slightly.The alterations in the Sollingen claystone can be represented by the global reaction (unbalanced) shown in Eqn (2).

$$\underset{\text{Illite}}{K_{0.6}Mg_{0.25}Al_{2.3}Si_{3.5}O_{10}(OH)_2} + \underset{\text{clinochlore}}{Mg_5Al_2Si_3O_{10}(OH)_8} + CO_2 + H_2O + Ca^{2+} \rightleftharpoons \underset{\text{K-feldspar}}{K\,AlSi_3O_8} + \underset{\text{kaolinite}}{Al_2Si_2O_5(OH)_4} + \underset{\text{dolomite}}{CaMgCO_3} + Mg^{2+}\# \quad (2)$$

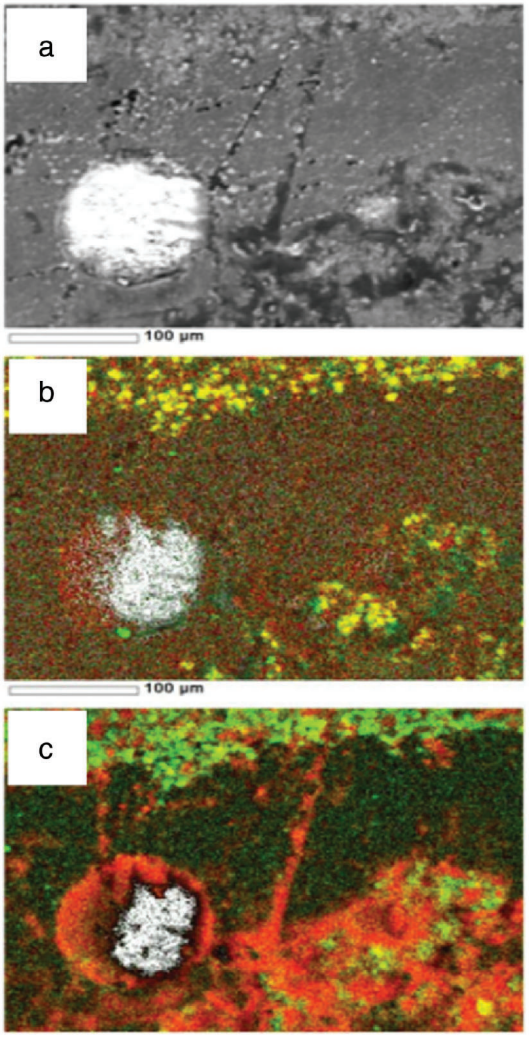

Figure 10. Secondary electron map of a proposed shear zone in the Sollingen sample (A) elemental map of the corresponding area for magnesium (red) and calcium (green) (B), elemental map of the corresponding area for silicon (red) and aluminum (green) (C).

In the Röt claystone, besides the common alterations mentioned earlier, there is a significant formation of albite (not visible in Fig. 12 due to scale), reaching 1.42 mmol (from starting 1.14 mmol, a 24,5% increase. After ca. 4000 years, illite is completely dissolved, reducing the supply of K to form K-feldspar. Since no dolomite is formed, the Mg released from illite and clinochlore dissolution remains in solution, increasing significantly its concentration (Fig. 12B). The overall process for the Röt claystone can be represented by Eqn (3).

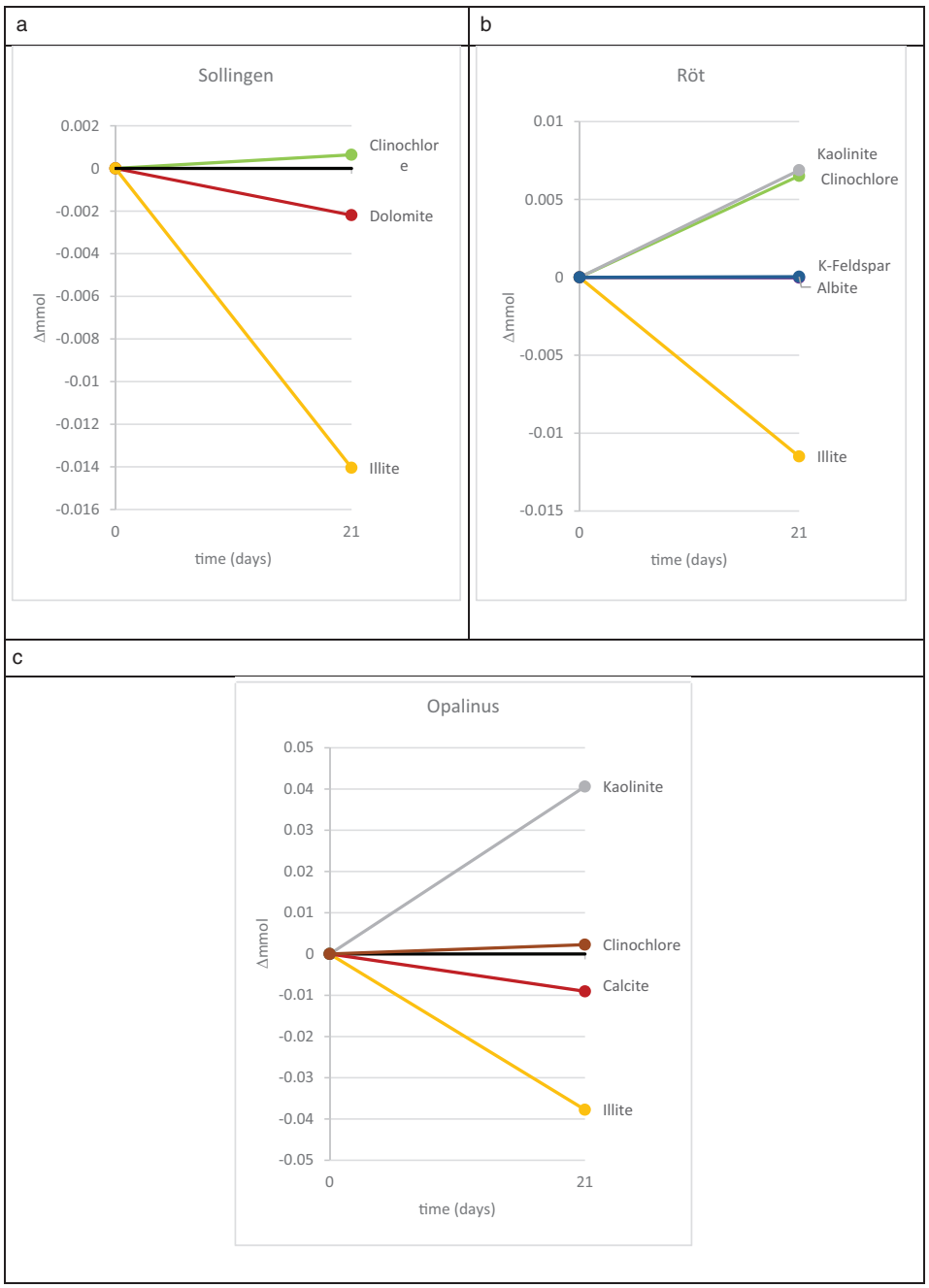

Figure 11. Mineral amount variations during 21-day reaction simulation with A) Sollingen; B) Röt and C) Opalinus samples.

$$\underset{\text{illite}}{K_{0.6}Mg_{0.25}Al_{2.3}Si_{3.5}O_{10}(OH)_2} + \underset{\text{clinochlore}}{Mg_5Al_2Si_3O_{10}(OH)_8} + CO_2 + H_2O \rightleftharpoons \underset{\text{K-feldspar}}{KAlSi_3O_8} + \underset{\text{albite}}{NaAlSi_3O_8} + \underset{\text{kaolinite}}{Al_2Si_2O_5(OH)_4} + Mg^{2+}\# \quad (3)$$

Carbonates are more strongly affected in the Opalinus claystone—approximately 50% of the initial calcite is dissolved, and a large amount of dolomite is formed (ca. 4 mmol). Dolomite formation consumes the Mg released by illite and clinochlore dissolution, but not completely, as its concentration in solution increases

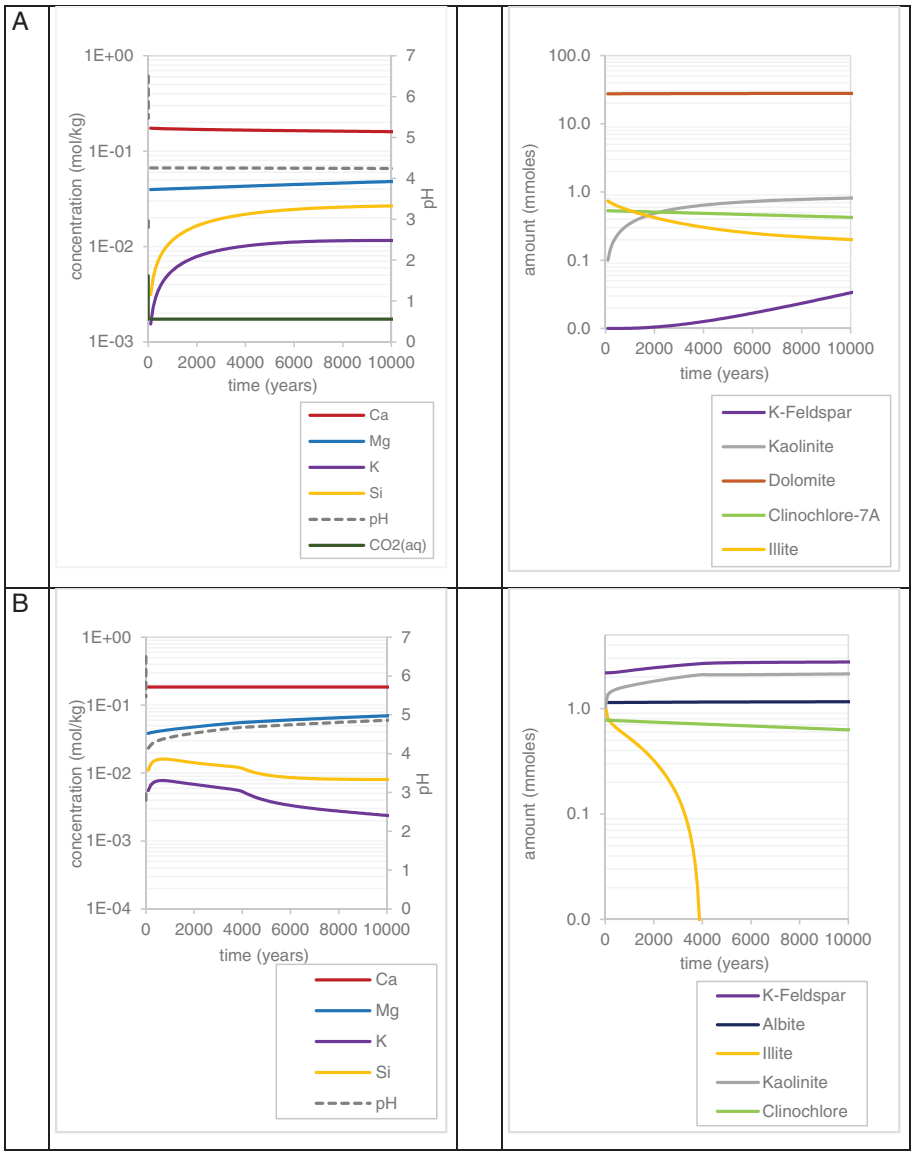

Figure 12. Variation of pH and element concentration (log scale) in solution (left column) and mineral amounts (log scale, right column) during 10 000-year dissolution and precipitation kinetics simulation with Solligen (A), Röt (B) and Opalinus (C) samples.

continuously. Illite dissolves completely in ca. 2300 years, stopping the supply of K and further precipiation of K-feldspar. Equation 4 represent the global alterations of the Opalinus composition.

$$\underset{\text{illite}}{K_{0.6}Mg_{0.25}Al_{2.3}Si_{3.5}O_{10}(OH)_2} + \underset{\text{clinochlore}}{Mg_5Al_2Si_3O_{10}(OH)_8} + \underset{\text{calcite}}{CaCO_3} + CO_2 + H_2O \rightleftharpoons \underset{\text{dolomite}}{CaMgCO_3} + \underset{\text{K-feldspar}}{KAlSi_3O_8} + \underset{\text{kaolinite}}{Al_2Si_2O_5(OH)_4} + Mg^{2+}\# \quad (4)$$

Discussion

In this section the experimental results obtained from the present study and its limitations will be discussed.

Crushed sample experiments

In the crushed sample experiments, there is an overall increase in the aqueous concentration of cations (Ca^{2+}, Mg^{2+}, K^{2+}) after reaction, resulting from the dissolution favored by the fine particles from the crushing procedure.

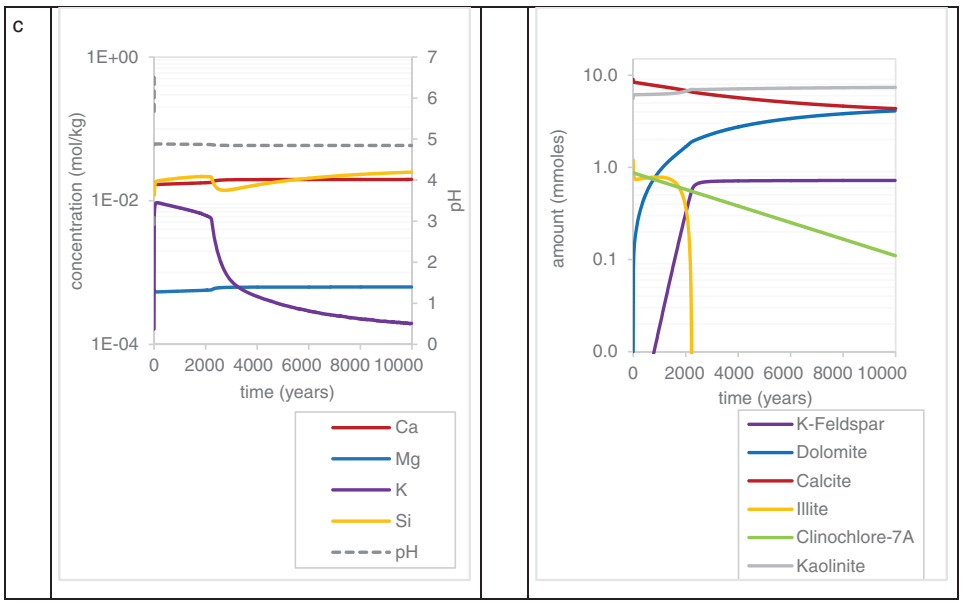

Figure 12. *Continued*

Chemical composition analyses before and after reaction show that illite dissolution must occur, as indicated by the potassium appearance after reaction, as illite is the only possible source for this cation and no potassium is present in the initial solution. This is further confirmed by the numerical simulations, where illite dissolves in the 21-day simulation of the experiments.

Numerical modeling

The observed alterations in the short-term kinetic models are overall in agreement with the experimental results for the crushed undeformed sample reactions, where increases in Ca, Mg, and K in solution were registered, which may have originated either from carbonates (Ca, Mg) or illite and clinochlore dissolution (K, Mg). In the long-term simulations, these trends are mostly continued. It should be kept in mind that the 21 days simulation was finished with cooling and depressurization of the system, which restores circumneutral/basic pH and may affect final results (while the 10 000-year simulations end with system under constant high pCO_2 and a pH between 4–5). Fast illite dissolution is favored in all the samples and conditions, at the very beginning of the process, even despite the high salinity of the medium. This dissolution appears to be in agreement with chemical analyses after the experiments (K^+ increase). Illite dissolution has been shown to occur in previous studies of CO_2-water-rock interactions,[10,44] yet in some cases precipitation was observed and also modeled, as well as the illitization of smectites.[19,45]

Overall, as a result of the simulations, the clays in the rocks (illite and chlorite) seem to be transformed into kaolinite and K-feldspar. This was already observed in similar modeling studies[16] Ketzer et al.;[48] Alemu et al.[49]).

It should be mentioned that modeling clay-water interactions has limitations and results have to be considered carefully. Not only the rate parameters for the kinetic simulations are important, but also the specific clays that are chosen to be included in the model to represent the sample composition. Also, the number of secondary minerals included in the model is usually limited and must be well defined—a large number of minerals might hinder kinetic calculations for longer times. Chemical structures of clays are hardly well established, and the chemical formula that represents a given clay mineral in thermodynamics databases can be significantly different from the real sample to be modeled, mostly due to variations in the relative amounts of cations present in the clay interlayers. Finally, clay mineral reactive surface area can vary orders of magnitude, as the measurements are strongly dependent on the method, as well as the source and preparation of the sample.

Sheared plates

Although the appearance of the band observed in this study is consistent with a shear band, the band or the

precipitates found within it could be an artifact caused by the leaching.[46] This would explain the relatively high amounts of silicon found within the proposed shear bands as quartz minerals are relatively inert and would be a residue of this process. Another explanation is that the small grain size made the fault gouge more fragile and the material has been lost to erosional processes during pressurization leaving behind a void.[47] If this would be the case it would be expected that more resin would be present within the bands, showing as a higher signal for carbon and oxygen on the EDS. This however was not the case for most of the shear bands. Due to the fine grain size of the material and the limitations of the SEM, it was not possible to detect a grain size decrease within the shear bands.

Conclusions

After reacting crushed material from three different caprock formations with CO_2-saturated brine under geological storage conditions, only minor alterations were found in the caprock mineralogy. It is important to note that in an effective seal, only minute amounts of brine will penetrate the caprock, making the water-rock ratio very small. The observed alterations are mostly consistent between the chemical analyses and numerical models, showing an overall increase in cation concentrations (Ca^{2+}, K^{+}, Mg^{2+}) coming from dissolution of clays (illite and chlorite) and carbonates. Long-term numerical simulation, however, suggest that alterations can be more extensive, with illite and chlorite being transformed into kaolinite and K-feldspar over 10 000 years. Carbonates are only affected more strongly in the Opalinus claystone. Surprisingly, the carbonate rich Sollingen is the least altered in the simulated period.

After the experiment with a method for reacting fault gauge material with CO_2-saturated brine using autoclaves, some shear bands were successfully identified. In one of the shear bands, precipitation of some sort was found providing evidence that the shear band had functioned as a preferential pathway for the CO_2-saturated brine.

Over the timespan of the experiment, the Opalinus clay behaved quasi inert when exposed to CO_2-saturated brine. Overall, experimental results show no indications that the geochemical sealing of Opalinus would be affected by CO_2 injection. We found rapid dissolution of dolomite occurring in the Sollingen claystone. Depending on reactive transport, dissolution can lead to significant porosity increases in the dolomite-rich formation. In the case of a well-functioning seal, mineral alterations should be limited to the first meters. As preexisting faults are present only in the 10 m-thick Sollingen deposits, increased dolomite dissolution in fault gouge might cause leakage through the formation. The P15-8 gas field situated in the Netherlands sector of the North Sea, for example, is overlain by a thick group (200 m) of consecutive caprock formations including both Sollingen and Röt claystone. Short-term mineral alterations identified in this study are not likely to be a threat for the geochemical sealing capabilities of the Röt formation. Furthermore, for the Sollingen formation, cementation by secondary dolomite and precipitation of secondary kaolinite might lead to reductions in permeability.

After the experiments with sheared sample casings, some shear bands were successfully identified. In one of the shear bands some precipitation was observed providing evidence that the shear band had functioned as a preferential pathway for the CO_2-saturated brine, allowing it to penetrate into the sample.

To better understand the effects of long-term CO_2 storage on existing fault regimes, fault zone alterations need to be closer examined. A lot of research has been performed on the effect of temperature, wetting and pore pressure differences on the friction coefficient. However, the effects of mineral alterations that will take place over longer time periods are not well known. By performing wet shear experiments in the presence of CO_2, letting the CO_2 react with the powder and after some time continuing the shear experiment under the same conditions, it should be possible to determine whether mineral alterations affect slip behavior.

Acknowledgments

This study was financed in part by the Coordenação de Aperfeiçoamento de Pessoal de Nível Superior - Brasil (CAPES) - Finance Code 001.

References

1. IPCC, in *Special Report on Carbon Dioxide Capture and Storage*, ed. by Metz B, Davidson O, de Coninck H, Loos M and Meyer L. Intergovernmental Panel on Climate Change, New York (2005).
2. Ketzer JM, Iglesias RS and Einloft S, Reducing greenhouse gas emissions with CO2 capture and geological storage, in *Handbook of Climate Change Mitigation and Adaptation*. 2nd edn. ed. by Chen W-Y, Suzuki T, and Lackner M. Springer

New York, New York pp. 1–40 (2015). https://doi.org/10.1007/978-1-4614-6431-0_37-2.

3. White CM, Strazisar BR, Granite EJ, Hoffman JS and Pennline HW, Separation and capture of CO_2 from large stationary sources and sequestration in geological formations - Coalbeds and deep saline aquifers. *J Air Waste Manage Assoc* **53**:645–715 (2003).
4. Bachu S, Screening and ranking of sedimentary basins for sequestration of CO2 in geological media in response to climate change. *Environ Geol* **44**:277–289 (2003).
5. Bachu S, CO_2 storage in geological media: Role, means, status and barriers to deployment. *Prog Energy Combust Sci* **34**(2):254–273 (2008). https://doi.org/10.1016/j.pecs.2007.10.001.
6. Neij L, Cost development of future technologies for power generation—A study based on experience curves and complementary bottom-up assessments. *Energy Policy* **36**(6):2200–2211 (2008). https://doi.org/10.1016/j.enpol.2008.02.029.
7. Kohler E, Parra T, Brosse E, Tocque E and Dubacq B, Cap-rock alteration in CO2-H2O medium: experimental approach of clays behavior. Paper presented at American Association of Petroleum Geologists Annual Convention, Houston, TX, pp. 57–58 (2006).
8. Credoz A, Bildstein O, Jullien M, Raynal J, Pétronin J-C, Lillo M*et al.* Experimental and modeling study of geochemical reactivity between clayey caprocks and CO_2 in geological storage conditions. *Energy Procedia* **1**:3445–3452 (2009). https://doi.org/10.1016/j.egypro.2009.02.135.
9. Kohler E, Parra T and Vidal O, Clayey cap-rock behavior in H2O-CO2 media at low pressure and temperature conditions: an experimental approach. *Clays Clay Miner* **57**:616–637 (2009). Available at: http://ccm.geoscienceworld.org/content/57/5/616.abstract.
10. Bildstein O, Kervévan C, Lagneau V, Delaplace P, Crédoz A, Audigane P *et al.* Integrative modeling of caprock integrity in the context of CO2 storage: Evolution of transport and geochemical properties and impact on performance and safety assessment. *Oil Gas Sci Technol* **65**:485–502 (2010). Available at: http://doi.org/10.2516/ogst/2010006.
11. Wollenweber J, Alles S, Busch A, Krooss BM, Stanjek H and Littke R, Experimental investigation of the CO_2 sealing efficiency of caprocks. *Int J Greenhouse Gas Control* **4**(2):231–241 (2010). https://doi.org/10.1016/j.ijggc.2010.01.003.
12. Samuelson J and Spiers CJ, Fault friction and slip stability not affected by Co 2 storage : evidence from short-term laboratory experiments on North Sea reservoir sandstones and caprocks. *Int J Greenhouse Gas Control* **11**:S78–S90 (2012). https://doi.org/10.1016/j.ijggc.2012.09.018.
13. Amann-Hildenbrand A, Bertier P, Busch A and Krooss BM, Experimental investigation of the sealing capacity of generic clay-rich caprocks. *Int J Greenhouse Gas Control* **19**:620–641 (2013). https://doi.org/10.1016/j.ijggc.2013.01.040.
14. Smith MM, Sholokhova Y, Hao Y and Carroll SA, Evaporite caprock integrity: an experimental study of reactive mineralogy and pore-scale heterogeneity during brine-CO(2) exposure. *Environ Sci Technol* **47**(1):262–268 (2013). https://doi.org/10.1021/es3012723.
15. Kampman N, Busch A, Bertier P, Snippe J, Hangx S and Pipich V, Observational evidence confirms modelling of the long-term integrity of CO_2-reservoir caprocks. *Nat Commun* **7**:12268 (2016). Available at: http://doi.org/10.1038/ncomms12268.
16. Gaus I, Azaroual M and Czernichowski-Lauriol I, Reactive transport modelling of the impact of CO_2 injection on the clayey cap rock at Sleipner (North Sea). *Chem Geol* **217**:319–337 (2005). https://doi.org/10.1016/j.chemgeo.2004.12.016.
17. Taberner C, Zhang G, Xu T and Cartwright L, Injection of supercritical CO_2 into deep saline carbonate formations. Predictions from geochemical modeling, in *EUROPEC/EAGE Conference and Exhibition*, Society of Petroleum Engineers, Amsterdam, the Netherlands, p. 11 (2009). https://doi.org/10.2118/121272-MS.
18. Shukla R, Ranjith P, Haque A and Choi S-KX, A review of studies on CO_2 sequestration and caprock integrity. *Fuel* **89**: 2651–2664 (2010). doi: https://doi.org/10.1016/j.fuel.2010.05.012.
19. de Lima V, Einloft S, Ketzer JM, Jullien M, Bildstein O and Petronin J-C, CO2 Geological storage in saline aquifers: Paraná Basin caprock and reservoir chemical reactivity. *Energy Procedia* **4**:5377–5384 (2011). https://doi.org/10.1016/j.egypro.2011.02.521.
20. Siqueira TA, Iglesias RS and Ketzer JM, Carbon dioxide injection in carbonate reservoirs – a review of CO_2-water-rock interaction studies. *Greenhouse Gases: Sci Technol* **7**(5):802–816 (2017). https://doi.org/10.1002/ghg.1693.
21. Bakker E, Kaszuba J, den Hartog S and Hangx S, Chemo-mechanical behavior of clay-rich fault gouges affected by CO2-brine-rock interactions. *Greenhouse Gases: Sci Technol* **9**(1):19–36 (2019). https://doi.org/10.1002/ghg.1831.
22. Geluk MC, Triassic, in *Geology of the Netherlands*, ed. by Wong TE, Batjes DAJ and Jager J. Royal Netherlands Academy of Arts and Sciences, Amsterdam, the Netherlands, pp. 85–106 (2007).
23. Arts RJ, Vandeweijer VP, Hofstee C, Pluymaekers MPD, Loeve D, Kopp A *et al.* The feasibility of CO_2 storage in the depleted P18-4 gas field offshore the Netherlands (the ROAD project). *Int J Greenhouse Gas Control* **11**:S10–S20 (2012). https://doi.org/10.1016/j.ijggc.2012.09.010.
24. Bossart P, Bernier F, Birkholzer J, Bruggeman C, Connolly P, Dewonck S *et al.* Mont Terri rock laboratory, 20 years of research: introduction, site characteristics and overview of experiments. *Swiss J Geosci* **110**(1):3–22 (2017). https://doi.org/10.1007/s00015-016-0236-1.
25. Gautschi A, Hydrogeology of a fractured shale (Opalinus Clay): Implications for deep geological disposal of radioactive wastes. *Hydrogeol J* **9**(1):97–107 (2001). https://doi.org/10.1007/s100400000117.
26. Thury M, The characteristics of the Opalinus clay investigated in the Mont Terri underground rock laboratory in Switzerland. *C R Phys* **3**(7):923–933 (2002). doi: https://doi.org/10.1016/S1631-0705(02)01372-5.
27. Iglesias RS, Bressan LW and Ketzer JM, Armazenamento geológico de carbono em aqüíferos salinos e campos de petróleo: geoquímica do sistema CO2-água-rocha através de experimentos e modelagem numérica, in *Mudanças Climáticas, Sequestro e Mercado de Carbono no Brasil*, ed. by Ziliotto MA. Curitiba, Curitiba, Brazil, pp. 203–217 (2009).
28. Pearson FJ, Arcos D, Bath A, Boisson JY, Fernández AM, Gäbler HE, Gaucher E, Gautschi A, Griffault L, Hernán P and Waber HN, Mont Terri project – geochemistry of water in the

Opalinus clay formation at the Mont Terri Rock laboratory. *Geology Series* (2003).

29. Koroleva M, Lerouge C, Mäder U, Claret F and Gaucher EC, Biogeochemical processes in a clay formation in situ experiment: part B – results from overcoring and evidence of strong buffering by the rock formation. *Appl Geochem* **26**(6):954–966 (2011). https://doi.org/10.1016/j.apgeochem.2011.03.005.
30. Gunter WD, Wiwchar B and Perkins EH, Aquifer disposal of CO_2-rich greenhouse gases: extension of the time scale of experiment for CO_2-sequestering reactions by geochemical modelling. *Mineral Petrol* **59**:121–140 (1997).
31. Lin H, Fujii T, Takisawa R, Takahashi T and Hashida T, Experimental evaluation of interactions in supercritical CO_2/water/rock minerals system under geologic CO_2 sequestration conditions. *J Mater Sci* **43**:2307–2315 (2008). Available at: http://doi.org/10.1007/s10853-007-2029-4.
32. Gysi AP and Stefánsson A, CO_2-water–basalt interaction. Low temperature experiments and implications for CO_2 sequestration into basalts. *Geochim Cosmochim Acta* **81**:129–152 (2012). https://doi.org/10.1016/j.gca.2011.12.012.
33. Parkhurst DL and Appelo CAJ, User's guide to PHREEQC (version 2)—A computer program for speciation, batch-reaction, one-dimensional transport, and inverse geochemical calculations. Water-Resources Investigations Report. Denver, CO. U.S. Geological Survey Water Resources Investigations. doi: Rep. 99-4259 (1999).
34. Lasaga AC, Chemical Kinetics of Water-Rock Interactions. *J Geophys Res* **89**:4009–4025 (1984). https://doi.org/10.1029/JB089iB06p04009.
35. Palandri JL and Kharaka YK, A compilation of rate parameters of water-mineral interaction for application to geochemical modeling. *Open File Report*. Menlo Park, CA: U.S. Department of the Interior (2004).
36. Tester JW, Worley WG, Robinson BA, Grigsby CO and Feerer JL, Correlating quartz dissolution kinetics in pure water from 25 to 625°C. *Geochim Cosmochim Acta* **58**:2407–2420 (1994). https://doi.org/10.1016/0016-7037(94)90020-5.
37. Kohut CK and Warren CJ, Chlorites in *Soil Mineralogy with Environmental Applications*, ed. by Dixon JB and Schulzepp DG. Soil Science Society of America, Madison, WI, pp. 531–553 (2002). doi: https://doi.org/10.2136/sssabookser7.c17.
38. Klajmon M, Havlová V, Červinka R, Mendoza A, Franců J and Berenblyum R, REPP-CO_2: equilibrium modelling of CO_2-rock-brine systems. *Energy Procedia* **114**:3364–3373 (2017). https://doi.org/10.1016/j.egypro.2017.03.1468.
39. Macht F, Eusterhues K, Pronk GJ and Totsche KU, Specific surface area of clay minerals: comparison between atomic force microscopy measurements and bulk-gas (N2) and -liquid (EGME) adsorption methods. *Appl Clay Sci* **53**:20–26 (2011). https://doi.org/10.1016/j.clay.2011.04.006.
40. Hellevang H, Aagaard P, Oelkers EH and Kvamme B, Can Dawsonite permanently trap CO_2? *Environmental Science & Technology* **39**:8281–8287 (2005). https://doi.org/10.1021/es0504791.
41. Köhler SJ, Dufaud F and Oelkers EH, An experimental study of illite dissolution kinetics as a function of ph from 1.4 to 12.4 and temperature from 5 to 50°C. *Geochim Cosmochim Acta* **67**(19):3583–3594 (2003). https://doi.org/10.1016/S0016-7037(03)00163-7.
42. Pham VTH, Lu P, Aagaard P and Hellevang H, On the potential of CO2-water-rock interactions for CO_2 storage using a modified kinetic model. *Int J Greenhouse Gas Control* **5**:1002–1015 (2011). https://doi.org/10.1016/j.ijggc.2010.12.002.
43. Pluymakers AMH, Peach CJ and Spiers CJ, Diagenetic compaction experiments on simulated anhydrite fault gouge under static conditions. *J Geophy Res: Solid Earth* **119**(5):4123–4148 (2014). https://doi.org/10.1002/2014JB011073.
44. Pruess K, Tsang C-F, Law DH-S and Oldenburg CM, An Intercomparison Study of Simulation Models for Geologic Sequestration, in *1st National Conference on Carbon Sequestration*. Washington, DC (2001).
45. Credoz A, Bildstein O, Jullien M, Raynal J, Trotignon L and Pokrovsky O, Mixed-layer illite–smectite reactivity in acidified solutions: Implications for clayey caprock stability in CO_2 geological storage. *Appl Clay Sci* **53**(3):402–408 (2011). https://doi.org/10.1016/j.clay.2011.01.020.
46. Hangx SJT and Spiers CJ, Reaction of plagioclase feldspars with CO_2 under hydrothermal conditions. *Chem Geol* **265**:88–98 (2009). https://doi.org/10.1016/j.chemgeo.2008.12.005.
47. Cladouhos TT, Shape preferred orientations of survivor grains in fault gouge. *J Struct Geol* **21**(4):419–436 (1999). https://doi.org/10.1016/S0191-8141(98)00123-0.
48. Ketzer JM, Iglesias RS, Einloft S, Dullius J, Ligabue R and de Lima V, Water-Rock-CO_2 interactions in saline aquifers aimed for carbon dioxide storage: Experimental and numerical modeling studies of the rio bonito formation (permian), Southern Brazil. *Applied Geochemistry* **24**(5):760–767 (2009).
49. Alemu BL, Aagaard P, Munz IA and Skurtveit E, Caprock interaction with CO_2: A laboratory study of reactivity of shale with supercritical CO_2 and brine. *Applied Geochemistry* **26**:1975–1989 (2011).

Roland Vernooij

Roland Vernooij has a MSC degree on energy science from Utrecht University. He is currently a PhD-candidate at the Vrije Universiteit Amsterdam where he uses drones to measure greenhouse gas and aerosol emissions and studies the drivers of variability in biomass burning emission factors in the savanna biome.

Tiago de Abreu Siqueira

Tiago de Abreu Siqueira is graduated in Chemistry, and has his PhD in Materials Engineering and Techonology at Pontifical Catholic University of Rio Grande do Sul - PUCRS. Presently working as Researcher in geochemical experimental modeling and coordinator of Geochemical Analyses Lab at Institute of Petroleum and Natural Resources (IPR – PUCRS).

Suzanne Hangx

Suzanne Hangx is an assistant professor at the High Pressure and Temperature Laboratory at Utrecht University. She studies the physical and chemical processes controlling rock mechanical behaviour in the subsurface, in the context of CO_2/energy storage and geo-energy production.

Christopher Spiers

Christopher Spiers is Emeritus Professor at the High Pressure and Temperature Laboratory at Utrecht University. He researches the mechanical behavior of rocks and faults, and the controlling microphysics, under the conditions that pertain in the Earth's crust.

Marcelo Ketzer

Marcelo Ketzer is a geologist and professor at the Department of Biology and Environmental Science, Linnaeus University, Sweden. His current research interests are on the chemistry of sediments (and related pore waters and gases) in their pristine state and when altered by human activities, and on the response of natural systems to climate change.

Rodrigo Sebastian Iglesias

Rodrigo Sebastian Iglesias is graduated in Chemistry at Federal University of Rio Grande do Sul (1997), has a Master's degree in Theoretical Chemistry at Federal University of Rio Grande do Sul (2000) and Doctorate in Organic Chemistry at Universidad Autonoma de Madrid (2006). Currently working as Associate Professor at the School of Technology at PUCRS, researching on geochemical experimental and numerical modeling at the Institute of Petroleum and Natural Resources at PUCRS.

